Flutter and Limit Cycle Oscillations of Cantilevered Plate in Supersonic Flow

Article *in* Journal of Aircraft · November 2020

DOI: 10.2514/1.C035992

Flutter and Limit Cycle Oscillations of Cantilevered Plate in Supersonic Flow

Kevin A. McHugh,* Maxim Freydin,* and Kai Kruger Bastos*
Duke University, Durham, North Carolina 27708
Philip Beran†
U.S. Air Force Research Laboratory, Wright–Patterson Air Force Base, Ohio 45433
and
Earl H. Dowell‡
Duke University, Durham, North Carolina 27708

https://doi.org/10.2514/1.C035992

Research interest is growing for theoretical models of highly deflected structures in aeroelastic settings. Presented here is a model of a cantilevered plate subjected to axial supersonic flow to determine the flutter boundary and postflutter characteristics of a system such as a trailing edge control surface. The structural model is a nonlinear inextensible beam model with inertia and stiffness geometric nonlinearities, while the aerodynamic model used is both first-order linear and third-order nonlinear Piston Theory with a new geometric modification to account for large deflections of the cantilevered configuration. Comparisons are made between linear and nonlinear structural models as well as linear and nonlinear Piston Theory, with and without this new geometric modification. It is shown that the model is highly sensitive to the inclusion of each nonlinear aerodynamic or structural component and that the new geometric modification to Piston Theory leads to stable limit cycles which otherwise may be unstable. Finally, the use of Piston Theory for these unconventionally large deflections is validated by comparing pressures on the structure to those computed by the Euler equations acting on the structure's prescribed motion.

Nomenclature

b	=	width of plate
EI	=	flexural rigidity of plate
h	=	thickness of plate
L	=	length of plate
M_∞	=	freestream Mach number
m	=	mass per unit length of plate
P_∞	=	freestream pressure
U_∞	=	freestream velocity
u	=	longitudinal deflection
w	=	transverse deflection
$\dot{x}$	=	time derivative
x'	=	spatial derivative
β	=	angle of deflected plate to freestream
γ	=	ratio of specific heats
Δp	=	pressure across plate
$\delta W^{NC_{\text{aero}}}$	=	virtual work due to aerodynamics
δ_β	=	delta function set to 0 or 1 indicating without or with β effect
Λ	=	compliance ratio
λ	=	constraint force
μ	=	mass ratio
Ψ	=	mode shape

I. Introduction

AEROELASTICITY of thin plates in supersonic flow is currently generating much research interest. Recently, Spottswood et al. [1] have conducted experimental tests of a thin plate clamped on all four sides subjected to supersonic flow and have demonstrated nonlinear limit cycle oscillations (LCO) as well as buckling behavior. Freydin et al. [2] modeled a similar system of a clamped plate with thermal stresses. In addition, Currao et al. [3] have measured experimental pressures on and deflections of a cantilevered plate in supersonic flow well below the flutter boundary and with a shock impinging on the plate. This configuration is of interest for modeling engineering structures such as trailing edge control surfaces on supersonic and hypersonic aircraft. Although the geometry in this case is simplified significantly from a genuine control surface, the investigation of clamped-free boundary conditions of a thin, flat plate offers valuable insights into the fluid–structure interaction, stability, and effectiveness of these more complex systems.

It is therefore our aim to provide theory and modeling to coincide with this recent advancement of experimental work and to push ahead into the postflutter regime for a cantilevered plate subjected to axial flow. Presented here is a compact, nonlinear computational model for cantilevered plates in axial supersonic flow using the inextensible beam structural theory along with Piston Theory aerodynamic theory. The inextensible beam model has been chosen as it is a good approximation for largely deflected structures which have fixed-free boundary conditions and may be easily coupled with Piston Theory to develop a highly efficient computational aeroelastic model.

The equations of motion for nonlinear inextensible beams have been studied in the literature in various contexts, and Lacarbonara [4] provides a clear overview of several methods of enforcing inextensibility. Notably, several studies have used Lagrange's equations to model the beam [5–8]. Crespo da Silva and Glynn [7,8] used a Lagrange multiplier to enforce the inextensibility constraint, a method similar to what is presented herein. These approaches, however, are tailored toward analytical solutions to stability problems and use perturbation methods or harmonic balance to solve for stability criteria. Here, we use a modal analysis and Runge–Kutta time-marching scheme to evaluate the dynamics of the system in the time domain.

Recent advances by us and our colleagues in nonlinear beam and plate theory and accompanying computations demonstrate a capability to model the responses of these structures with high computational efficiency [9–15]. Tang et al. [9] derived new, nonlinear equations of motion for largely deflected, inextensible beams and extended this formulation to plates. Dowell and McHugh [11]

Received 4 May 2020; revision received 6 July 2020; accepted for publication 12 July 2020; published online 30 October 2020.

*Department of Mechanical and Materials Science, Box 90300 Hudson Hall.
†Principle Research Aerospace Engineer, 2210 Eighth Street B146. Associate Fellow AIAA.
‡William Holland Hall Professor, Department of Mechanical Engineering and Materials Science, Honorary Fellow AIAA.

derived similar equations for the inextensible beam using Hamilton's principle, but used a Lagrange multiplier to enforce the inextensibility constraint. Using the Rayleigh–Ritz approach to expand these equations modally, they demonstrated the method's abilities to model both cantilever and free–free beam dynamics [13]. Recently, McHugh and Dowell [14] validated their model's ability to capture flutter points by adding a static follower point-force load to the tip of a cantilevered beam and solving for the flutter and limit cycle behavior of this configuration, well known as Beck's beam problem [16].

In the present Paper, the same inextensible beam theory has been used as in the study of the dynamics and stability of the system under a follower load [14], but now the follower force is replaced by an aerodynamic theory appropriate to high-speed flows. The classic text on Hypersonic Flow Theory by Hayes and Probstein [17] has an insightful discussion of how, in inviscid flow at sufficiently high Mach number, each plane section normal to the freestream can be modeled independently of one another. This law of plane sections was exploited by Lighthill [18] in his well-known paper and later formalized as an aeroelastic tool by Ashley and Zartarian [19] to develop what is known as Piston Theory.

Piston Theory is used throughout the literature for high-speed potential flow [9–22] and is relevant to contemporary studies in supersonic configurations [3,22]. Notably, Currao et al. [3] recently showed that Piston Theory effectively captures the dynamics of a cantilevered beam in hypersonic flow below the onset of flutter, and Nydick et al. [20] performed an admirable study in which first- and third-order Piston Theory were used to compute the aeroelastic LCO response of a pinned–pinned panel in hypersonic flow. Although these results indicate that third-order Piston Theory matches well with Euler results, they also suggest that viscous effects have a large damping effect on the results "because the surface motion occurs mainly within the boundary layer." The cantilevered boundary conditions in the present Paper allow for the surface motion to be much greater than a typical boundary layer thickness, so it is assumed that an inviscid flow treatment will be adequate.

Work is ongoing in the field to increase the accuracy of the Piston Theory method. It is natural to use either experimental or computational [computational fluid dynamics (CFD)] information for steady flow over a wing or body to determine the local flow properties at any given streamwise section and replace the freestream parameters in the Piston Theory with these local values. This has been done by Scott and Pototzky [23], and Zhang et al. [24] demonstrated that this Local Piston Theory matches results from an Euler CFD solver better than Classical Piston Theory. Meijer and Dala [25] make the point that the usual nonlinear version of Piston Theory as given by Lighthill [18] can be used in the same fashion. Brouwer and McNamara [26] note that changes in the mean flow ahead and behind a shock can also be taken into account as long as the Mach numbers ahead of and behind the shock are sufficiently greater than 1. Brouwer and McNamara have also used Piston Theory as the starting point for obtaining a system identification model using CFD data to account for flow separation. Recently Shi et al. [27] and Meng et al. [28] have discussed how a fully nonlinear Piston Theory might be constructed by using the full wave expansion or shock expansion models as discussed in the classic text by Liepmann and Roshko [29]. Finally, it is noted that Dowell and Bliss [30,31] have considered how Piston Theory may be generalized by starting from linear potential flow theory and expanding that solution in powers of inverse Mach number squared or inverse frequency squared. Starting from potential flow theory, Piston Theory is the correct limit at high Mach for all frequencies or at high frequencies for all Mach numbers, although the latter limit is not as well known. Expansion in inverse powers of Mach allow Piston Theory to be used at lower (supersonic) Mach number, which may be useful in practice.

In the present Paper, Piston Theory is advanced by the use of a new addition to Classical Piston Theory [both linear (first order) and nonlinear (third order)] to account for the fact that at large deflections the aerodynamic pressure must act normal to the instantaneously deformed surface of the structure. In the prior literature, the pressure defined by Piston Theory is applied perpendicular to the freestream flow regardless of the angle the airfoil takes to the undisturbed flow. Because the cantilevered conditions allow for large deflections of the structure, a new geometric modification to Piston Theory is introduced here. With use of the parameter $\beta(x)$ (the angle of the beam with respect to its undeformed horizontal datum), the pressure is always applied normal to the instantaneous shape of the beam. Moreover, the accuracy of the new Piston Theory is assessed by comparing the results of Piston Theory with those of Euler based CFD simulations. Thus, the emphasis in this Paper is on the aerodynamic model per se and the consequences of this model (in combination with inextensible beam theory) for determining the flutter and limit cycle oscillations of the system.

The present model then includes four nonlinearities: two structural and two aerodynamic. Although the effects of the structural geometric nonlinearities alone have been reported previously by us [13,14], the aerodynamic nonlinearities are novel, and certainly the interplay among the four nonlinearities proves to be interesting and important. It is found that the geometric modification to Piston Theory introduces a further aerodynamic nonlinearity and increases the stability of the model. It is also found that third-order nonlinear Piston Theory predicts a higher limit cycle amplitude than the first-order linear theory.

Also note that when modeling any physical system and certainly a fluid–structural (aeroelastic) system it is important to study the sensitivity of the results to different model attributes. Here, we identify three types of sensitivities which are significant to this Paper. Type 1 is the sensitivity to the mathematical model of the physical system. How do the results change when new mathematics are introduced to the system? Type 2 is the sensitivity to the parameters that appear in the mathematical model or which are considered in the design of an experimental model. How do the results change based on varying geometric or material properties of the structure or the freestream flow properties? Type 3 is the accuracy of the numerical methods employed to extract solutions from the mathematical model. This is typically measured by performing a convergence study. Each of these is considered in the present Paper.

Finally, a word about the nomenclature of beam or plate may be useful. Formally, the configuration is a plate with no spanwise bending. Because the structure is assumed to be clamped along its entire leading edge, and the panel width is on the order of the panel chord, the structure bends principally in the streamwise direction, and thus the bending in the spanwise direction is negligible. Reference [10] considers a similar structural configuration in low-speed, subsonic flow in a combined experimental/theoretical study. As shown in Ref. [10], spanwise bending can be neglected in both the experimental and the theoretical model.

With regard to Piston Theory, whether first order or higher order, the effective aerodynamic aspect ratio is the product of $\sqrt{M^2-1} * (b/L)$, where b is the plate span and L is the plate chord. Thus, even for a square plate with $b/L = 1$, the aerodynamic aspect ratio will be large for the Mach number range of interest to the present Paper. On the other hand, if b/L is sufficiently small for a given M, then three-dimensional aerodynamic effects might be included. Yet, one might still invoke the essential Piston Theory assumption of the transverse plane of fluid at each chordwise position being independent of each other. But now the piston would have finite width.

Thus, the structure considered here has a finite width b, but because the factor b appears in both the structural model and aerodynamic model in proportion, it cancels and does not appear in the final results. If in future work spanwise bending is included in the structural model or finite aspect ratio effects are included in the aerodynamic model, then b and its nondimensional counterpart b/L will appear as another parameter to be considered.

II. Development of Governing Equations

A. Unforced Equations of Motion

A schematic of the cantilevered beam model in flow is shown in Fig. 1. The beam can deflect in the longitudinal u component as well as the transverse w component. The equations of motion for the unforced beam are derived in our recent work [13,14] from Lagrange's equations using the Rayleigh–Ritz method. That is, each

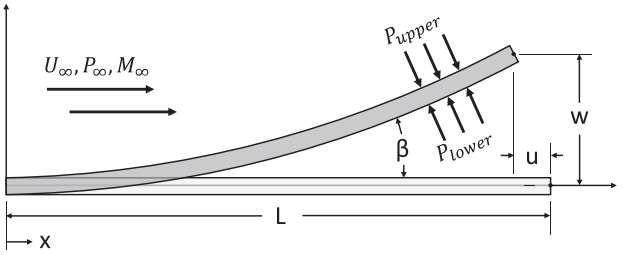

Fig. 1 Schematic of cantilevered beam with uniform flow over top and bottom surfaces.

component of deflection, u and w, as well as the constraint force λ are modally expanded as shown in the Appendix.

The equations of motion are reproduced here in dimensionless form:

$$\ddot{\boldsymbol{u}} - \boldsymbol{A}\boldsymbol{\lambda} = 0 \tag{1}$$

$$\ddot{\boldsymbol{w}} + 2\boldsymbol{\zeta}\boldsymbol{\omega}\dot{\boldsymbol{w}} + \boldsymbol{\omega}^2\boldsymbol{w} - \boldsymbol{B}\boldsymbol{w}\boldsymbol{\lambda} + \boldsymbol{P}\boldsymbol{w}^3 = 0 \tag{2}$$

$$\boldsymbol{u} + \frac{1}{2}\boldsymbol{A}^{-1}\boldsymbol{B}\boldsymbol{w}\boldsymbol{w} = 0 \tag{3}$$

A short nondimensionalization from the equations derived in Ref. [14] is shown in the Appendix, while a brief explanation of the equations terms is given here. Equation (1) is the equation for longitudinal deflection u, where λ is the internal constraint force to enforce inextensibility. Equation (2) is the equation for transverse deflection w, where ζ is the damping parameter and the final two terms are the nonlinear inertia and stiffness terms, respectively. Equation (3) is the constraint equation which couples the slope of the longitudinal deflection u to that of the transverse deflection w to enforce inextensibility. Note that u, w, and λ are all expressed in a modal series.

Each of the variables appear as boldface italic text, indicating that they are written in matrix form. The definition of each term and the transcriptions from index notation to matrix notation are shown in the following:

$$\overline{u}_i \equiv \frac{u_i}{L} \Rightarrow \boldsymbol{u}, \quad \overline{w}_j \equiv \frac{w_j}{L} \Rightarrow \boldsymbol{w}$$

$$\overline{\lambda_k} \equiv \frac{L^2}{EI}\lambda_k \Rightarrow \boldsymbol{\lambda}, \quad \overline{\omega_j} \equiv \left(\frac{mL^4}{EI}\right)^{1/2}\omega_j \Rightarrow \boldsymbol{\omega}$$

$$\overline{M}^u_{ii} \equiv \frac{M^u_{ii}}{L} \equiv \int_0^1 \Psi^u_i \Psi^u_i \,\mathrm{d}\xi \Rightarrow \boldsymbol{M_u}, \quad \overline{M}^w_{jj} \equiv \frac{M^w_{jj}}{L} \equiv \int_0^1 \Psi^w_j \Psi^w_j \,\mathrm{d}\xi \Rightarrow \boldsymbol{M_w}$$

$$\overline{A}_{ik} \equiv \int_0^1 \Psi^{u'}_i \Psi^\lambda_k \,\mathrm{d}\xi \Rightarrow \boldsymbol{A}, \quad \overline{B}_{kj_1j} \equiv LB_{kj_1j} \equiv \int_0^1 \Psi^\lambda_k \Psi^{w'}_{j_1} \Psi^{w'}_j \,\mathrm{d}\xi \Rightarrow \boldsymbol{B}$$

$$\overline{P}_{j_1j_2j_3j} \equiv L^5 P_{j_1j_2j_3j} \equiv \int_0^1 (\Psi^{w''}_{j_1}\Psi^{w''}_{j_2}\Psi^{w'}_{j_3}\Psi^{w'}_j + \Psi^{w''}_{j_1}\Psi^{w'}_{j_2}\Psi^{w'}_{j_3}\Psi^{w''}_j)\,\mathbf{d}\xi \Rightarrow \boldsymbol{P}$$

Note that the prime $'$ symbol represents $\partial/\partial x$. Therefore, when nondimensionalizing length, the following relationships are important:

$$x = L\xi \qquad \frac{\partial}{\partial x} = \frac{1}{L}\frac{\partial}{\partial \xi} \qquad \frac{\partial^2}{\partial x^2} = \frac{1}{L^2}\frac{\partial^2}{\partial \xi^2} \tag{4}$$

We can nondimensionalize time and its derivatives as follows, where the overlined terms are dimensionless:

$$t = \left(\frac{mL^4}{EI}\right)^{1/2}\bar{t} \quad \frac{\partial}{\partial t} = \left(\frac{EI}{mL^4}\right)^{1/2}\frac{\partial}{\partial \bar{t}} \quad \frac{\partial^2}{\partial t^2} = \frac{EI}{mL^4}\frac{\partial^2}{\partial \bar{t}^2} \tag{5}$$

A discussion of vector/matrix size and characteristics may be appropriate. Vectors $\boldsymbol{u}$, $\boldsymbol{w}$, and $\boldsymbol{\lambda}$ are length I, J, and K, respectively, where I, J, and K are the number of modes included in each component. Matrices $\boldsymbol{M_u}$ and $\boldsymbol{M_w}$ are diagonal matrices of size I^2 and J^2, respectively. Matrix $\boldsymbol{A}$ is of size $I \times K$. Tensor $\boldsymbol{B}$ is three dimensional of size $K \times J \times J$, and $\boldsymbol{P}$ is four dimensional of size J^4. Matrix $\boldsymbol{\omega}^2$ is a diagonal matrix with each nonzero entry as the square of the corresponding modal natural frequency.

B. Piston Theory Aerodynamic Forcing

Piston theory [18,19,21,22] provides a simple relation between pressure perturbation and motion of a structure, one side of which is under a freestream flow with properties $\rho_\infty, U_\infty, M_\infty$. Because our plate model has fluid acting on both sides, we calculate a change in pressure across the upper and lower surfaces:

$$p_{\text{upper}} = \frac{\rho_\infty U_\infty}{M_\infty}\left[\left(\dot{w} + U_\infty\frac{\partial w}{\partial x}\right) + \frac{\gamma+1}{4a_\infty}\left(\dot{w} + U_\infty\frac{\partial w}{\partial x}\right)^2 + \frac{\gamma+1}{12a_\infty^2}\left(\dot{w} + U_\infty\frac{\partial w}{\partial x}\right)^3\right]$$

$$p_{\text{lower}} = \frac{\rho_\infty U_\infty}{M_\infty}\left[\left(-\dot{w} - U_\infty\frac{\partial w}{\partial x}\right) + \frac{\gamma+1}{4a_\infty}\left(-\dot{w} - U_\infty\frac{\partial w}{\partial x}\right)^2 + \frac{\gamma+1}{12a_\infty^2}\left(-\dot{w} - U_\infty\frac{\partial w}{\partial x}\right)^3\right]$$

Note that x is positive in the flow direction. Now, we subtract the upper surface from the lower [21], and note the second-order terms cancel one another due to symmetry. However, this would not be the case for a plate with a nonzero initial angle of attack or initial curvature.

$$\Delta p = p_{\text{lower}} - p_{\text{upper}} = -2\frac{\rho_\infty U_\infty}{M_\infty}\left[\left(\dot{w} + U_\infty\frac{\partial w}{\partial x}\right) + \frac{\gamma+1}{12a_\infty^2}\left(\dot{w} + U_\infty\frac{\partial w}{\partial x}\right)^3\right] \tag{6}$$

The virtual work acting on the plate is given by

$$\delta W^{NC_{\text{aero}}} = \int_0^L b\Delta p\boldsymbol{n}\cdot\delta\boldsymbol{r}\,\mathrm{d}x \tag{7}$$

where $\boldsymbol{n}$ is the unit normal to the deflected plate and $\delta\boldsymbol{r}$ is the virtual displacement of the plate. Piston Theory is classically used to predict pressures only in the direction normal to the undeformed plate, which intrinsically assumes that the slopes are small. The virtual work would then be expressed as Eq. (8):

$$\delta W^{NC_{\text{aero}}} = \int_0^L b\Delta p\delta w\,\mathrm{d}x \tag{8}$$

For fully pinned or clamped plates, this assumption is valid. However, the small deflection assumption no longer holds for the case of a cantilevered plate, and therefore a large deflection expression must be derived.

1. *Large Deflection Correction*

Because of the large displacement of the beam, we understand that pressure must be everywhere normal to the deflected beam. Therefore, the pressure contributes to both the δu and δw components of the virtual work. To derive the correct form of the virtual work for this case, consider the beam with longitudinal deflection w in the $\boldsymbol{i}$ direction and transverse deflection u in $\boldsymbol{j}$. The virtual displacement is $\delta\boldsymbol{r} = \delta u\boldsymbol{i} + \delta w\boldsymbol{j}$, and the local tangent vector to the deformed beam is $\boldsymbol{\tau} = \cos\beta\boldsymbol{i} + \sin\beta\boldsymbol{j}$, where β is the angle of the beam relative to the undeformed horizontal. Now, the local normal to the deformed beam is $\boldsymbol{n} \equiv k \times \boldsymbol{\tau} = -\sin\beta\boldsymbol{i} + \cos\beta\boldsymbol{j}$, and by incorporating this into Eq. (7), the expression for virtual work is given by Eq. (9):

$$\delta W^{NC_{\text{aero}}} = \int_0^L [-b\Delta p\sin(\beta)\delta u + b\Delta p\cos(\beta)\delta w]\,\mathrm{d}x \tag{9}$$

Note that $\sin\beta$ and $\cos\beta$ are defined from geometric relationships as follows:

$$\tan\beta = \frac{(\partial w/\partial x)}{1+(\partial u/\partial x)} = \frac{w'}{1+u'} = \frac{w'}{1-1/2w'^2} \equiv f \tag{10}$$

$$\tan\beta = \frac{\sin\beta}{\cos\beta} = f \tag{11}$$

$$\sin^2\beta + \cos^2\beta = 1 \tag{12}$$

$$f^2 = \frac{\sin^2\beta}{\cos^2\beta} \tag{13}$$

So, then,

$$(f^2+1)\cos^2\beta = 1 \tag{14}$$

$$\cos\beta = \frac{1}{(f^2+1)^{1/2}} \tag{15}$$

From this, we can find $\sin\beta$ as well:

$$\sin\beta = \frac{f}{(f^2+1)^{1/2}} \tag{16}$$

Now, substituting Eq. (10) into Eqs. (15) and (16), we can write the definitions of $\sin\beta$ and $\cos\beta$ in terms of w:

$$\cos\beta = (1-w'^2)^{1/2} \approx (1-1/2w'^2) \tag{17}$$

$$\sin\beta = w' \tag{18}$$

So, the expression for virtual work acting on the plate [Eq. (9)] can be written as follows:

$$\delta W^{NC_{\text{aero}}} = \int_0^L b\Delta p(-w'\delta u + (1-1/2w'^2)\delta w)\,\mathrm{d}x \tag{19}$$

2. First-Order Piston Theory

For first-order Piston Theory, we neglect the third-order term in Eq. (6), so the change in pressure across the beam is the classical result

$$\Delta p = -2\frac{\rho_\infty U_\infty}{M_\infty}\left(\dot{w} + U_\infty\frac{\partial w}{\partial x}\right) \tag{20}$$

Substituting Eq. (20) into Eq. (19), scaling length and time with Eqs. (4) and (5), and multiplying both sides by L/EI to nondimensionalize, the expression for nondimensional virtual work is as follows:

$$\frac{L}{EI}\delta W^{NC_{\text{aero}}} = -\int_0^1 2b\frac{\rho_\infty L}{M_\infty m}\left(U_\infty\left(\frac{mL^2}{EI}\right)^{1/2}\frac{\partial\overline{w}}{\partial\overline{t}} + \frac{mL^2U_\infty^2}{EI}\frac{\partial\overline{w}}{\partial\xi}\right) \times\left(-\frac{\partial\overline{w}}{\partial\xi}\delta\overline{u} + (1-1/2\left(\frac{\partial\overline{w}}{\partial\xi}\right)^2)\delta\overline{w}\right)\mathrm{d}\xi \tag{21}$$

Now, we can use the following nondimensional parameters to simplify the equation. Note that μ is the aerodynamic to structural mass ratio and Λ is the aerodynamic to structural compliance ratio and both incorporate the Mach number in their definition:

$$\mu \equiv \frac{\rho_\infty bL}{mM_\infty} \tag{22}$$

$$\Lambda \equiv \frac{\rho_\infty U_\infty^2 bL^3}{EIM_\infty} \tag{23}$$

$$(\Lambda\mu)^{1/2} = \frac{\rho_\infty U_\infty bL^2}{M_\infty(EIm)^{1/2}} \tag{24}$$

$$\frac{L}{EI}\delta W^{NC_{\text{aero}}} = 2\int_0^1\left[\left((\Lambda\mu)^{1/2}\frac{\partial\overline{w}}{\partial\overline{t}}\frac{\partial\overline{w}}{\partial\xi} + \Lambda\left(\frac{\partial\overline{w}}{\partial\xi}\right)^2\right)\delta\overline{u} + \left(-(\Lambda\mu)^{1/2}\frac{\partial\overline{w}}{\partial\overline{t}} - \Lambda\frac{\partial\overline{w}}{\partial\xi} + \frac{1}{2}(\Lambda\mu)^{1/2}\frac{\partial\overline{w}}{\partial\overline{t}}\left(\frac{\partial\overline{w}}{\partial\xi}\right)^2 + \frac{1}{2}\Lambda\left(\frac{\partial\overline{w}}{\partial\xi}\right)^3\right)\delta\overline{w}\right]\mathrm{d}\xi \tag{25}$$

Now, we can show that several of these terms are orders of magnitude smaller than others, and therefore negligible. To show this, we can scale $\partial\overline{w}/\partial\overline{t}$ by $\omega\overline{w}$:

$$\frac{L}{EI}\delta W^{NC_{\text{aero}}} = 2\int_0^1\left[\left((\Lambda\mu)^{1/2}\omega\overline{w}\frac{\partial\overline{w}}{\partial\xi} + \Lambda\left(\frac{\partial\overline{w}}{\partial\xi}\right)^2\right)\delta\overline{u} + \left(-(\Lambda\mu)^{1/2}\omega\overline{w} - \Lambda\frac{\partial\overline{w}}{\partial\xi} + \frac{1}{2}(\Lambda\mu)^{1/2}\omega\overline{w}\left(\frac{\partial\overline{w}}{\partial\xi}\right)^2 + \frac{1}{2}\Lambda\left(\frac{\partial\overline{w}}{\partial\xi}\right)^3\right)\delta\overline{w}\right]\mathrm{d}\xi \tag{26}$$

Lastly, we note the order of each term, using the physical geometries and properties given in the Appendix:

$$\mu = \mathcal{O}[10^{-4}]$$
$$\Lambda = \mathcal{O}[10^{2}]$$
$$\overline{\omega} = \mathcal{O}[10^{1}]$$
$$\overline{w} = \mathcal{O}[10^{-1}]$$
$$\frac{\partial\overline{w}}{\partial\xi} = \mathcal{O}[10^{-1}]$$

This approximation then leads to the following orders of magnitude[§]:

$$\frac{L}{EI}\delta W^{NC_{\text{aero}}} = 2\int_0^1[(\mathcal{O}[10^{-2}] + \mathcal{O}[10^{0}])\delta\overline{u} + (-\mathcal{O}[10^{-1}] - \mathcal{O}[10^{1}] + \mathcal{O}[10^{-3}] + \mathcal{O}[10^{-1}])\delta\overline{w}]\,\mathrm{d}\xi \tag{27}$$

It should be no surprise that the largest term comes from the classical linear Piston Theory, which corresponds to having no β effect, i.e. when $\beta = 0$. However, it is notable that the second term in the u coordinate is so large. For now, we will neglect the terms of order $\mathcal{O}[10^{-2}]$; or higher. Therefore, the final form of the nonlinear follower-style first-order Piston Theory virtual work becomes the following.

$$\frac{L}{EI}\delta W^{NC_{\text{aero}}} = 2\int_0^1\left[\Lambda\left(\frac{\partial\overline{w}}{\partial\xi}\right)^2\delta\overline{u} + \left(-(\Lambda\mu)^{1/2}\frac{\partial\overline{w}}{\partial\overline{t}} - \Lambda\frac{\partial\overline{w}}{\partial\xi} + \frac{\Lambda}{2}\left(\frac{\partial\overline{w}}{\partial\xi}\right)^3\right)\delta\overline{w}\right]\mathrm{d}\xi \tag{28}$$

Now, substitute the following modal expansions of w and u [Eqs. (A4) and (A5) in the Appendix] into Eq. (28):

[§]Note that a formal ordering scheme can be developed by expanding the solution in terms of the fluid to structural mass ratio, which is a small parameter, typically 0.01 or smaller. The result to first order is the same as in the Paper. As shown in Fig. 9, the results are very insensitive to the mass ratio for small mass ratios.

$$\frac{L}{EI}\delta W^{NC_{\text{aero}}} = 2\int_0^1 \left[\Lambda \sum_{j1}\sum_{j2} \Psi_{j1}^{w'}\Psi_{j2}^{w'} w_{j1} w_{j2}\delta\left(\sum_i \Psi_i^u u_i\right)\right.$$
$$+\left(-(\Lambda\mu)^{1/2}\sum_{j1}\Psi_{j1}^{w}\dot{w}_{j1} - \Lambda\sum_{j1}\Psi_{j1}^{w'} w_{j1}\right.$$
$$\left.\left.+\frac{\Lambda}{2}\sum_{j1}\sum_{j2}\sum_{j3}\Psi_{j1}^{w'}\Psi_{j2}^{w'}\Psi_{j3}^{w'} w_{j1} w_{j2} w_{j3}\right)\delta\left(\sum_j \Psi_j^w w_j\right)\right]\mathrm{d}\xi \quad (29)$$

$$\frac{L}{EI}\delta W^{NC_{\text{aero}}} = 2\sum_i\left(\Lambda\sum_{j1}\sum_{j2}\int_0^1 \Psi_i^u\Psi_{j1}^{w'}\Psi_{j2}^{w'}\,\mathrm{d}\xi w_{j1} w_{j2}\right)\delta u_i$$
$$+2\sum_j\left(-(\Lambda\mu)^{1/2}\sum_{j1}\int_0^1 \Psi_j^w\Psi_{j1}^{w}\,\mathrm{d}\xi\dot{w}_{j1} - \Lambda\sum_{j1}\int_0^1 \Psi_j^w\Psi_{j1}^{w'}\,\mathrm{d}\xi w_{j1}\right.$$
$$\left.+\frac{\Lambda}{2}\sum_{j1}\sum_{j2}\sum_{j3}\int_0^1 \Psi_j^w\Psi_{j1}^{w'}\Psi_{j2}^{w'}\Psi_{j3}^{w'}\,\mathrm{d}\xi w_{j1} w_{j2} w_{j3}\right)\delta w_j \quad (30)$$

Now, we can concisely write the integrals in our matrix form:

$$D_{ijj1} = \int_0^1 \Psi_i^u\Psi_j^{w'}\Psi_{j1}^{w'}\,\mathrm{d}\xi \Rightarrow \boldsymbol{D} \quad (31)$$

$$G_{j1j2j3j} = \frac{1}{2}\int_0^1 \Psi_j^w\Psi_{j1}^{w'}\Psi_{j2}^{w'}\Psi_{j3}^{w'}\,\mathrm{d}\xi \Rightarrow \boldsymbol{G} \quad (32)$$

$$H_{jj1} = \int_0^1 \Psi_j^w\Psi_{j1}^{w'}\,\mathrm{d}\xi \Rightarrow \boldsymbol{H} \quad (33)$$

And finally, the virtual work can be concisely written as follows:

$$\frac{L}{EI}\delta W^{NC_{\text{aero}}} = 2\sum_i(\Lambda \boldsymbol{D}\boldsymbol{w}\boldsymbol{w})\delta u_i$$
$$+2\sum_j(-(\Lambda\mu)^{1/2}\boldsymbol{M}\dot{\boldsymbol{w}} - \Lambda\boldsymbol{H}\boldsymbol{w} + \Lambda\boldsymbol{G}\boldsymbol{w}\boldsymbol{w}\boldsymbol{w})\delta w_j \quad (34)$$

Now, using Eq. (A3) to extract the nonconservative force in each coordinate and using Eq. (A1) to apply the forces to Eqs. (1) and (2), we get the following set of equations including the aerodynamic forces. Note that the terms which originated from our new β modification are noted by multiplying by a scalar δ_β, which can be set to 1 for calculations which include the β effect or zero for calculations which omit the β effect:

$$\ddot{\boldsymbol{u}} - \boldsymbol{A}\boldsymbol{\lambda} = 2\delta_\beta\Lambda\boldsymbol{D}\boldsymbol{w}^2 \quad (35)$$

$$\ddot{\boldsymbol{w}} + 2\boldsymbol{\zeta}\omega\dot{\boldsymbol{w}} + \omega^2\boldsymbol{w} - \boldsymbol{B}\boldsymbol{w}\boldsymbol{\lambda} + \boldsymbol{P}\boldsymbol{w}^3$$
$$= -2(\Lambda\mu)^{1/2}\dot{\boldsymbol{w}} - 2\Lambda\boldsymbol{H}\boldsymbol{w} + 2\delta_\beta\Lambda\boldsymbol{G}\boldsymbol{w}^3 \quad (36)$$

$$\boldsymbol{u} + \frac{1}{2}\boldsymbol{A}^{-1}\boldsymbol{B}\boldsymbol{w}\boldsymbol{w} = 0 \quad (37)$$

3. Third-Order Piston Theory

The next step is to continue the expansion of Piston Theory to the third-order form. We can rearrange Eq. (6) as follows:

$$\Delta p = -2\frac{\rho_\infty U_\infty}{M_\infty}\left(\dot{w} + U_\infty\frac{\partial w}{\partial x}\right)\left[1 + \frac{\gamma+1}{12}\left(\frac{\dot{w}}{a_\infty} + M_\infty\frac{\partial w}{\partial x}\right)^2\right] \quad (38)$$

By assuming that $((\dot{w}/a_\infty) + M_\infty(\partial w/\partial x))^2$ is small compared to 1, we arrive at Eq. (20). However, if this term is not sufficiently small, it should be included in our formulations.

To demonstrate the scale of this term, we first simplify and rearrange the terms in brackets:

$$\Delta p = -2\frac{\rho_\infty U_\infty}{M_\infty}\left(\dot{w} + U_\infty\frac{\partial w}{\partial x}\right)\left[1 + \frac{M_\infty^2(\gamma+1)}{12}\left(\frac{\dot{w}}{U_\infty} + \frac{\partial w}{\partial x}\right)^2\right] \quad (39)$$

Nondimensionalizing the terms in brackets allows their comparison with respect to 1:

$$\left[1 + \frac{M_\infty^2(\gamma+1)}{12}\left(\left(\frac{\mu}{\Lambda}\right)^{1/2}\dot{\overline{w}} + \frac{\partial\overline{w}}{\partial\xi}\right)^2\right]$$

Finally, if $\dot{\overline{w}}$ scales with characteristic frequency, we are left with the following:

$$\left[1 + \frac{M_\infty^2(\gamma+1)}{12}\left(\left(\frac{\mu}{\Lambda}\right)\overline{\omega}^2\overline{w}^2 + 2\left(\frac{\mu}{\Lambda}\right)^{1/2}\overline{\omega}\,\overline{w}\frac{\partial\overline{w}}{\partial x} + \left(\frac{\partial\overline{w}}{\partial x}\right)^2\right)\right]$$

Again, we note the order of each term:

$$M_\infty = \mathcal{O}[1]$$
$$\mu = \mathcal{O}[10^{-4}]$$
$$\Lambda = \mathcal{O}[100]$$
$$\overline{\omega} = \mathcal{O}[10]$$
$$\overline{w} = \mathcal{O}[10^{-1}]$$
$$\frac{\partial\overline{w}}{\partial\xi} = \mathcal{O}[10^{-1}]$$

This approximation then leads to the following orders of magnitude:

$$[1 + \mathcal{O}[10^{-6}] + \mathcal{O}[10^{-4}] + \mathcal{O}[10^{-2}]]$$

Note that in our original derivation we keep the $(\partial w/\partial x)^2$ term, so we will keep it here, but disregard the higher-order terms. So, the third-order Piston Theory may be appropriately simplified as follows:

$$\Delta p = -2\frac{\rho_\infty U_\infty}{M_\infty}\left(\dot{w} + U_\infty\frac{\partial w}{\partial x}\right)\left[1 + \frac{M_\infty^2(\gamma+1)}{12}\left(\frac{\partial w}{\partial x}\right)^2\right] \quad (40)$$

Note that the third-order Piston Theory pressure is always larger than that given by first-order theory and this leads to larger amplitude limit cycle oscillations. We can include the third-order Piston Theory terms in the equation of motion by beginning again with Eq. (9) and substitute Eq. (40) into Δp:

$$\delta W^{NC_{\text{aero}}} = \int_0^L -b\Delta p\sin(\beta)\delta u + b\Delta p\cos(\beta)\delta w\,\mathrm{d}x$$
$$= -\int_0^L\left[2b\frac{\rho_\infty U_\infty}{M_\infty}\left(\frac{\partial w}{\partial t} + U_\infty\frac{\partial w}{\partial x}\right)\left[1 + \frac{M_\infty^2(\gamma+1)}{12}\left(\frac{\partial w}{\partial x}\right)^2\right]\right.$$
$$\left.\times(-\sin(\beta)\delta u + \cos(\beta)\delta w)\right]\mathrm{d}x \quad (41)$$

To reduce the complexity of the full equations, we can use the steps already taken in the first-order Piston Theory scaling analysis to truncate any higher-order terms. By similar analysis, the following can be shown:

$$\frac{L}{EI}\delta W^{NC_{\text{aero}}} = -\int_0^1\left[2\mu\left(\left(\frac{\Lambda}{\mu}\right)^{1/2}\frac{\partial\overline{w}}{\partial\overline{t}} + \frac{\Lambda}{\mu}\frac{\partial\overline{w}}{\partial\xi}\right)\right.$$
$$\times\left[1 + \frac{M_\infty^2(\gamma+1)}{12}\left(\frac{\partial\overline{w}}{\partial\xi}\right)^2\right]$$
$$\left.\times\left(-\frac{\partial\overline{w}}{\partial\xi}\delta\overline{u} + \left(1 - 1/2\left(\frac{\partial\overline{w}}{\partial\xi}\right)^2\right)\delta\overline{w}\right)\right]\mathrm{d}\xi \quad (42)$$

$$\frac{L}{EI}\delta W^{NC_{\text{aero}}} = 2\int_0^1 \Bigg[\Bigg((\Lambda\mu)^{1/2}\frac{\partial \overline{w}}{\partial \overline{t}}\frac{\partial \overline{w}}{\partial \xi} + \Lambda\left(\frac{\partial \overline{w}}{\partial \xi}\right)^2 + (\Lambda\mu)^{1/2}\frac{M_\infty^2(\gamma+1)}{12}\frac{\partial \overline{w}}{\partial \overline{t}}\left(\frac{\partial \overline{w}}{\partial \xi}\right)^3 + \Lambda\frac{M_\infty^2(\gamma+1)}{12}\left(\frac{\partial \overline{w}}{\partial \xi}\right)^4\Bigg)\delta\overline{u} + \Bigg(-(\Lambda\mu)^{1/2}\frac{\partial \overline{w}}{\partial \overline{t}} - \Lambda\frac{\partial \overline{w}}{\partial \xi} + \frac{1}{2}(\Lambda\mu)^{1/2}\frac{\partial \overline{w}}{\partial \overline{t}}\left(\frac{\partial \overline{w}}{\partial \xi}\right)^2 + \frac{1}{2}\Lambda\left(\frac{\partial \overline{w}}{\partial \xi}\right)^3 - (\Lambda\mu)^{1/2}\frac{M_\infty^2(\gamma+1)}{12}\frac{\partial \overline{w}}{\partial \overline{t}}\left(\frac{\partial \overline{w}}{\partial \xi}\right)^2 + (\Lambda\mu)^{1/2}\frac{M_\infty^2(\gamma+1)}{24}\frac{\partial \overline{w}}{\partial \overline{t}}\left(\frac{\partial \overline{w}}{\partial \xi}\right)^4 - \Lambda\frac{M_\infty^2(\gamma+1)}{12}\left(\frac{\partial \overline{w}}{\partial \xi}\right)^3 + \Lambda\frac{M_\infty^2(\gamma+1)}{24}\left(\frac{\partial \overline{w}}{\partial \xi}\right)^5\Bigg)\delta\overline{w}\Bigg]\mathrm{d}\xi \tag{43}$$

This approximation then leads to the following orders of magnitude:

$$\frac{L}{EI}\delta W^{NC_{\text{aero}}} = 2\int_0^1 [(\mathcal{O}[10^{-2}] + \mathcal{O}[10^{0}] + \mathcal{O}[10^{-4}] + \mathcal{O}[10^{-2}])\delta\overline{u} + (-\mathcal{O}[10^{-1}] - \mathcal{O}[10^{1}] + \mathcal{O}[10^{-3}] + \mathcal{O}[10^{-1}] - \mathcal{O}[10^{-3}] + \mathcal{O}[10^{-5}] - \mathcal{O}[10^{-1}] + \mathcal{O}[10^{-3}])\delta\overline{u}]\mathrm{d}\xi \tag{44}$$

We can neglect any terms of order $\mathcal{O}[10^{-2}]$ or higher. So, the nonconservative work becomes the following:

$$\frac{L}{EI}\delta W^{NC_{\text{aero}}} = 2\int_0^1 \Bigg[\Lambda\left(\frac{\partial \overline{w}}{\partial \xi}\right)^2\delta\overline{u} + \Bigg(-(\Lambda\mu)^{1/2}\frac{\partial \overline{w}}{\partial \overline{t}} - \Lambda\frac{\partial \overline{w}}{\partial \xi} + \frac{1}{2}\Lambda\left(\frac{\partial \overline{w}}{\partial \xi}\right)^3 - \Lambda\frac{M_\infty^2(\gamma+1)}{12}\left(\frac{\partial \overline{w}}{\partial \xi}\right)^3\Bigg)\delta\overline{w}\Bigg]\mathrm{d}\xi \tag{45}$$

Again, substituting the modal expansions from Eqs. (A4) and (A5) yields the following:

$$\begin{aligned}\frac{L}{EI}\delta W^{NC_{\text{aero}}} = {} & 2\sum_i\Bigg(\Lambda\sum_{j1}\sum_{j2}\int_0^1 \Psi_i^u\Psi_{j1}^{w'}\Psi_{j2}^{w'}\,\mathrm{d}\xi w_{j1}w_{j2}\Bigg)\delta u_i \\ & + 2\sum_j\Bigg(-(\Lambda\mu)^{1/2}\sum_{j1}\int_0^1 \Psi_j^w\Psi_{j1}^{w}\,\mathrm{d}\xi\dot{w}_{j1} \\ & - \Lambda\sum_{j1}\int_0^1 \Psi_j^w\Psi_{j1}^{w'}\,\mathrm{d}\xi w_{j1} \\ & + \Lambda\left(1 - \frac{M_\infty^2(\gamma+1)}{6}\right)\frac{1}{2}\sum_{j1}\sum_{j2}\sum_{j3} \\ & \times\int_0^1 \Psi_j^w\Psi_{j1}^{w'}\Psi_{j2}^{w'}\Psi_{j3}^{w'}\,\mathrm{d}\xi w_{j1}w_{j2}w_{j3}\Bigg)\delta w_j\end{aligned} \tag{46}$$

Now, after transcribing the summation notation to our matrix notation, we have the following system of equations. Note that third-order Piston Theory only adds one term, a function of M_∞, which was not already accounted for by first-order Piston Theory. We will show that this term increases the pressure on the plate for a given Λ and M_∞:

$$\ddot{\boldsymbol{u}} - \boldsymbol{A}\boldsymbol{\lambda} = 2\delta_\beta\Lambda\boldsymbol{D}\boldsymbol{w}^2 \tag{47}$$

$$\ddot{\boldsymbol{w}} + 2\boldsymbol{\zeta}\boldsymbol{\omega}\dot{\boldsymbol{w}} + \boldsymbol{\omega}^2\boldsymbol{w} - \boldsymbol{B}\boldsymbol{w}\boldsymbol{\lambda} + \boldsymbol{P}\boldsymbol{w}^3 = -2(\Lambda\mu)^{1/2}\dot{\boldsymbol{w}} - 2\Lambda\boldsymbol{H}\boldsymbol{w} + 2\Lambda\left(\delta_\beta - \frac{M_\infty^2(\gamma+1)}{6}\right)\boldsymbol{G}\boldsymbol{w}^3 \tag{48}$$

$$\boldsymbol{u} + \frac{1}{2}\boldsymbol{A}^{-1}\boldsymbol{B}\boldsymbol{w}\boldsymbol{w} = 0 \tag{49}$$

III. Computational Methods

A. Modal Solution Method

Equations (47–49) are manipulated to form one equation for w, and this equation is solved with a fourth-order Runge–Kutta time-marching integration scheme. The three independent parameters Λ, μ, and M_∞ are set by physical properties of a proposed experimental setup, as discussed in the Appendix. Except for the cases where M_∞ and μ are varied, they are set to $M_\infty = 4$ and $\mu = 1 \times 10^{-4}$.

B. Euler Equation Validation Method

The geometrically modified Piston Theory aerodynamic model is validated for this configuration by comparison to the Euler equations computed with commercial CFD software. The fully nonlinear model coupled with third-order Piston Theory was used to generate unsteady beam response during limit cycle oscillation, in other words, past the flutter onset condition. The results were then used to prescribe wall motion in the computational domain. Five cases of freestream flow conditions are considered with static pressure parameter in the range of $67.75 \le \Lambda \le 71.75$, $M_\infty = 4$, and $\mu = 1 \times 10^{-4}$.

The cantilevered beam configuration was replicated in ANSYS FLUENT 19.2, where the beam was modeled as a one-dimensional zero-thickness line. A structured computational mesh was created in ANSYS ICEM CFD with a rectangular domain with dimensions as shown in Fig. 2 (the mesh was used in an unstructured solver). A total of 200 nodes along the beam were stationed with each node treated simultaneously as upper and lower surfaces using the ANSYS zero-thickness wall boundary condition. A user-defined function (UDF) was coded to prescribe the individual motion of each node according to its location on the beam and point in time. The UDF was activated by the Dynamic Mesh functionality of FLUENT with diffusive smoothing parameter set to 2. This resulted in a balanced motion of the mesh near and far from the beam and allowed for large deformations as shown in Fig. 2. The setting included a mesh of 215,000 nodes and a time step of $t = 6.1581 \times 10^{-5}$ s. Unsteady transients decayed after two structural limit cycles, where the first cycle was introduced to the mesh gradually using a linear (time-dependent) scaling factor.

Mesh density and time step convergence studies were conducted with second-order accurate implicit time integration and spatial discretization. The coupled pressure-based solver was used, and the Courant number, which in the Fluent coupled solver stabilizes the convergence behavior for each time step, was set to 5. Three mesh densities were considered with node count along the beam of 150, 200, and 300 with the rest of the mesh scaled accordingly. Three time steps were considered: $t_1 = 1.2316 \times 10^{-4}$ s, $t_2 = 6.1581 \times 10^{-5}$ s, and $t_3 = 3.0791 \times 10^{-5}$ s. Dual time stepping was employed, with a maximum of 200 subiterations per time step. Two domain sizes were considered: the smaller is shown in Fig. 2, while the larger had double the height and distance from beam trailing edge to the outlet. The edges of the domain were modeled as pressure-far-field, which sets a characteristic boundary condition using far-field temperature, pressure, and Mach number. Convergence was quantified by calculating the rms of pressure differential along the panel at several locations. The difference in pressure differential rms at 80% chord length between the finest case and that used for computations was less than 2% of the finest case value.

IV. Results and Their Sensitivity to Key Model Parameters

The results are presented in several sections to address several forms of sensitivites. First, we demonstrate the sensitivities to the number of modes and the time step for integration. Next, we present results which show sensitivities to the four key nonlinear modeling components: structural nonlinearities stiffness and inertia and aerodynamic nonlinearites due to higher (third-)order Piston Theory and the nonlinear geometric modification β. Finally, we present a sensitivity study of the key nondimensional parameters M_∞, Λ, and μ. We show that the model is highly sensitive to Λ, moderately sensitive to M_∞, but relatively insensitive to μ. However, recall that M_∞ also appears implicitly in the definitions of Λ and μ.

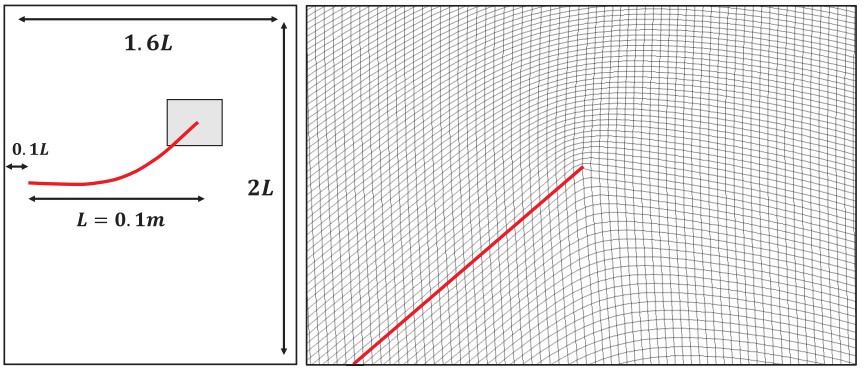

Fig. 2 Computational mesh domain with beam at maximum deflection and mesh distribution around tip of beam.

A. Sensitivity to Number of Modes and Time Step of Integration

After investigating several cases, it was determined that modal convergence was reached with $4w$, $6u$, and 6λ modes. Using any more than these modes, the results are not significantly changed (rms values differ less than 0.5%). It may be noted, however, that the time to complete a simulation grows with the number of w modes to the third power.

In addition, the time step was chosen as a constant in order to be more consistent across different cases when defining rms values. To determine the necessary time step, MATLAB®'s ode45 solver was employed to use its adaptive time stepping ability, and then an appropriately small time step was chosen based upon these results. Again, a smaller time step was shown not to improve accuracy of the scheme. For each computation, the time step was $\bar{t} = 0.0018$ (dimensionless time units).

B. Nonlinear Modeling Sensitivities

A fully linear fluid–structural model harmonically decays when perturbed from rest in a subcritical flow where flow parameters are below a stability boundary, and exponentially oscillates to (±) infinity in a supercritical flow. However, from our nonlinear theory, insights are gained from analyzing bounded limit cycle oscillations.

Originally, it was expected that the nonlinearities in the structural model would be strong enough to yield a bounded LCO due to First-Order Piston Theory. However, it can be seen in Fig. 3 that the LCO deflection response when normalized to beam length is much larger than 1, indicating that the model predicts behavior well beyond the physical system's realistic behavior. The results do, however, show an interesting phenomenon: that the initial conditions directly impact the flutter point. That is, for a small initial displacement of the beam $[w(0) = 0.0001]$, the flutter point is larger than for a higher initial condition $[w(0) = 0.01]$. This indicates a subcritical nonlinear bifurcation would occur at the flutter point of $\Lambda = 67.6$ and curve backward toward the first nonzero point on the open-circled curve at $\Lambda = 65.8$.

Introducing the geometric modification to Piston Theory (the β effect) ensures that the pressure acts always normal to the plate surface. By including the nonlinear aerodynamic terms which are functions of β for First-Order Piston Theory, the limit cycle oscillation is much smaller and physically credible. Indeed, even the linear structural model response is bounded when coupled with this new aerodynamic model. These results can be seen in Fig. 4, which plots the bifurcation diagram for several conditions and nonlinearities. Figure 4 includes the responses for the plate excited by First-Order Piston Theory and Third-Order Piston Theory with this new β effect included, and each aerodynamic model is considered with a fully nonlinear structural model and a linear structural model. Because of the large deflection of the plate, it can be seen that the Third-Order Piston Theory term is significant and increases the limit cycle amplitude. Also note that the nonlinear structural model increases the amplitude as well. This is due to the nonlinear inertia term dominating the nonlinear stiffness term. Finally, note the absence of any subcritical bifurcation.

To gain understanding of the sensitivities of the model to each of these different nonlinearities (aerodynamic and structural), cases were run with the several aerodynamic and structural terms either included or omitted. Table 1 concisely describes the limit cycle response of each case. The classification of *nonphysical* means that the response is not physically plausible because of excessive displacement, for example, $w/L > 1$. *Unbounded* signifies that the model's solution grows to infinity. *Supercritical* indicates that the LCO is stable for all Λ considered and the bifurcation is supercritical in nature, while *subcritical* indicates a stable LCO after a subcritical bifurcation, as seen in

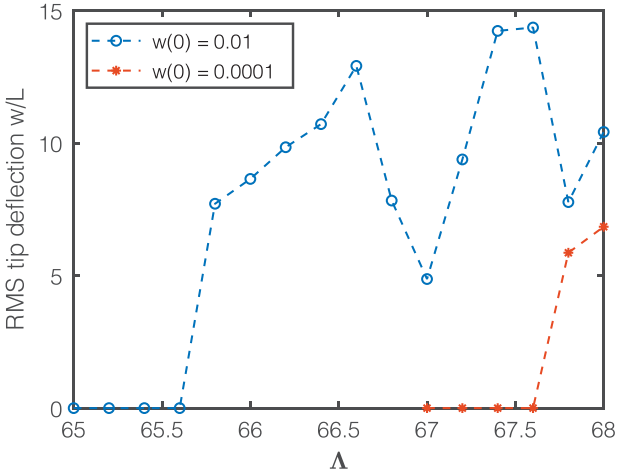

Fig. 3 LCO amplitudes vs aerodynamic forcing levels for first-order Piston Theory, $\delta_\beta = 0$, and fully nonlinear structure.

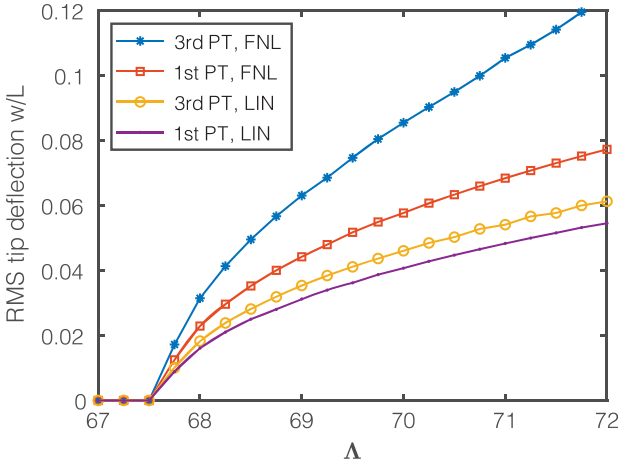

Fig. 4 LCO amplitudes vs aerodynamic forcing levels for third-order vs first-order nonlinear Piston Theory and linear or fully nonlinear structural models, $\delta_\beta = 1$.

Table 1 Limit cycle classifications for different Piston Theory nonlinearities vs structural nonlinearities

	Aerodynamics			
Structure	$\mathcal{O}1, \delta_\beta = 0$	$\mathcal{O}1, \delta_\beta = 1$	$\mathcal{O}3, \delta_\beta = 0$	$\mathcal{O}3, \delta_\beta = 1$
Full nonlinear	Nonphysical	Supercritical	Unbounded	Supercritical*
Nonlinear inertia	Nonphysical	Supercritical	Unbounded	Supercritical*
Nonlinear stiffness	Supercritical	Supercritical	Subcritical	Supercritical
Linear	— —	Supercritical	Subcritical	Supercritical

Figs. 3, 5, and 6. *Supercritical** designates that the limit cycle is bounded for a limited range of Λ and then grows to infinity for larger Λ.

It is of interest to understand physically why including the β effect (defining pressure to act normal to the instantaneous deformed shape of the plate) has a stabilizing effect on the LCO. Given the complexity of this nonlinear system, a simple explanation risks oversimplifying. However, it is noted that when the β effect is included the aerodynamic pressure components in the horizontal u direction are always positive. Thus, one may hypothesize that this leads to a tensile force in the x direction, which provides a stiffening effect to the beam. In addition, because the w component of pressure is multiplied by $\cos\beta$, the pressure levels in this component are lower at higher deflections than they would otherwise be without the β effect. It is some combination of the tensile effect in u and the diminished pressure in w which results in the stabilized LCO.

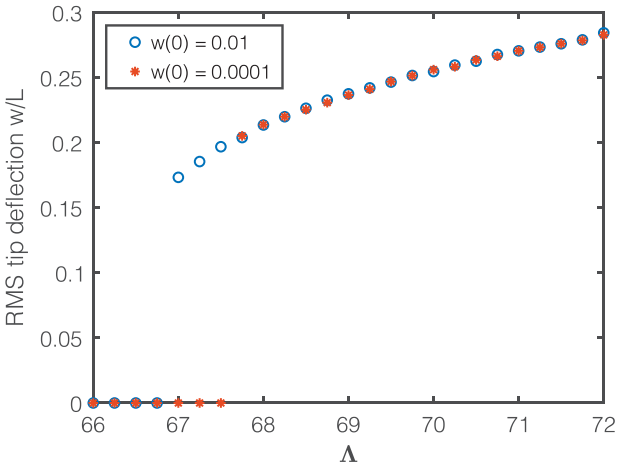

Fig. 5 LCO amplitudes vs aerodynamic forcing levels for third-order Piston Theory, $\delta_\beta = 0$, and nonlinear stiffness as the only structural nonlinearity.

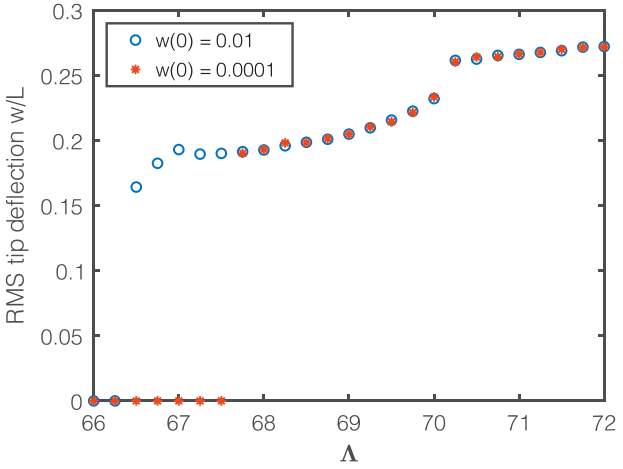

Fig. 6 LCO amplitudes vs aerodynamic forcing levels for third-order Piston Theory, $\delta_\beta = 0$, and a linear structural model.

The effects of the various structural nonlinearities are demonstrated in Fig. 7, which depicts the bifurcation diagram for Third-Order Nonlinear Piston Theory and $\delta_\beta = 1$. It can be seen that for the model with the inertia nonlinearity only (labeled *Inertia*) the amplitude is greatest. Opposing the inertia is the stiffness nonlinearity only case (labeled *Stiffness*), which when combined with the inertia only case becomes the fully nonlinear (*Full NL*) case. Note that the nonlinear stiffness only case is similar to the linear structural case, and the stiffness nonlinearity only seems to influence the system when the amplitudes become large. Also note that the fully nonlinear and inertia nonlinearity plots do not continue across the entire range of Λ values. The plots are stopped when the rms value is no longer bounded but instead extends to infinity. The point at which this occurs can be related to the point at which Piston Theory is no longer applicable more broadly, which will be discussed later.

C. Nondimensional Physical Parameter Sensitivity

We now consider how the physical system behaves with respect to key nondimensional parameters, μ, Λ, and M_∞. Each of these cases are run with Third-Order nonlinear Piston Theory with the β effect included ($\delta_\beta = 1$) and the fully nonlinear structural model. This is the most complete and physically realistic model considered in the present Paper.

The nondimensionalization of the equations results in the most compact and efficient way of determining sensitivity of the results to the various physical parameters. Note that a good choice of nondimensional parameters will reveal the order of importance of the nondimensional parameters. In our present Paper, the order is Λ (a ratio of aerodynamic to structural stiffness or compliance), M_∞ (Mach number), and μ (a ratio of fluid to structural mass).

Figure 8 illustrates the model's sensitivity to Λ and M_∞. Each curve pictures the limit cycle oscillation amplitude of a different Mach number flow as the fluid forcing Λ is increased. Note here the termination points of the plots for all flows. (Figure 8a is a zoomed-in plot of Fig. 8b to show the termination of responses for Mach 4, 5, and 6 flow.) Beyond the values of Λ for which no solution is plotted, the solutions diverge toward infinity. This is at a different value for each Mach number; however, it is calculated that each curve's

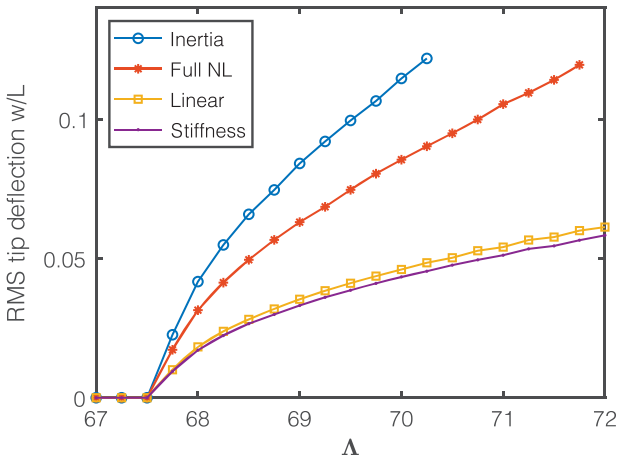

Fig. 7 LCO amplitudes vs aerodynamic forcing levels for third-order Piston Theory, $\delta_\beta = 1$.

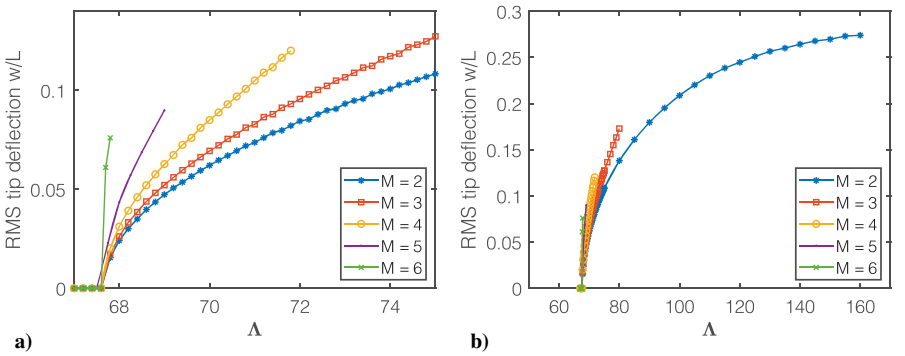

Fig. 8 LCO amplitudes vs aerodynamic forcing levels across several Mach numbers, all for third-order Piston Theory, $\delta_\beta = 1$, and fully nonlinear structure. Here, part a is a zoomed in plot of part b.

termination point occurs at $M_\infty *$ (RMS of tip deflection) ≈ 0.5. This is significant because classical Piston Theory is said to be valid for $M_\infty \delta < 0.5$, where δ is a measure of structural slope or angle of attack. See the discussion by Lighthill [18]. In addition, it is of practical significance to note that our model is limited in its predictions for high Mach number postcritical behavior.¶

Note also that, although Fig. 8 shows a strong dependence on Mach number, this is not the case for a model with only first-order Piston Theory included. For first-order Piston Theory, all of the effect of M_∞ is included in the definitions of μ and Λ, and there is no separate dependence on Mach number per se. Indeed, the bifurcation plots lay on top of one another for a first-order Piston Theory model.

Figure 9 shows that there is modest dependence on the mass ratio μ. The range of $1 \times 10^{-4} < \mu < 8 \times 10^{-4}$ was chosen based on appropriate physical values given in Appendix. B. For all other computations, a value of $\mu = 1 \times 10^{-4}$ is chosen.

V. Aerodynamic Model Validation

Because of the significant differences between first-order and third-order Piston Theory results in Fig. 4, one may question the accuracy of third-order Piston Theory. To answer this question, the pressures on the beam as calculated by Piston Theory in the fully nonlinear aeroelastic computation are compared to those calculated from the Euler equations using a prescribed motion on the beam from the same aeroelastic case at Mach 4. A representative solution from the Euler calculations is shown in Fig. 10, where $\Lambda = 71.75$ and the deflection is at a maximum. Note that a shock forms on the surface turned toward the flow. At large deflections, the beam becomes analogous to a ramp, and a strong shock forms on the deflected surface. This is characteristic of each of these simulations, but the following results show that this does not result in greatly different pressures from third-order Piston Theory, which interestingly is derived from the assumption that there are no shocks on the surface.

To compare Euler to Piston Theory, Fig. 11 illustrates the change in pressure calculated from the three theories across the beam's length at a given instance in time for various values of Λ. The time step chosen is when the deflection is largest in the cycle. Note that the quantity of interest is the pressure as calculated in the aeroelastic case. Since the pressure was calculated without the effect of the beam moving in the u direction, this effect is not included in these plots for the Piston Theory case. However, to compare to a higher-fidelity model, the u deflection is considered for the Euler computation. Therefore, these plots evaluate the Piston Theory method and its means of application.

To condense this information into one plot, Fig. 12 shows the maximum aerodynamic work Q_F done on the beam's surface as the forcing function (and therefore the deflection) increases. Aerodynamic

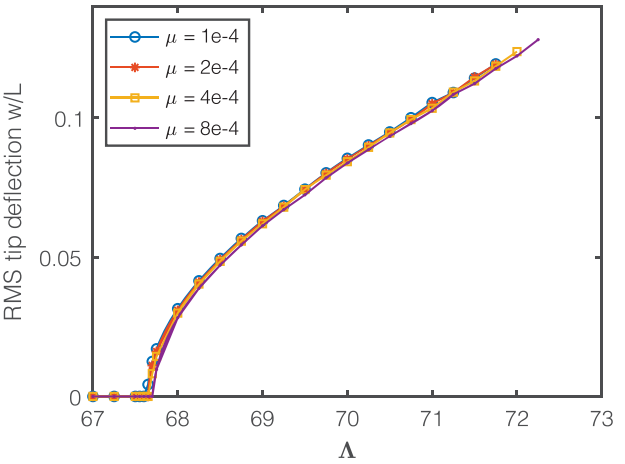

Fig. 9 LCO amplitudes vs aerodynamic forcing levels across several values of μ, all for third-order Piston Theory, $\delta_\beta = 1$, and fully nonlinear structure.

work is defined as $Q_F \equiv \int_0^L \Delta p(x) w_F(x)\,dx$ for the Piston Theory cases, where $w_F(x)$ is the vertical deflection of the beam at its peak deflection during a limit cycle oscillation. For the Euler case, aerodynamic work is defined as $Q_F \equiv \int_0^{L+u(L)} \Delta p(x+u)\hat{w}_F(x+u)\,dx$, where $\hat{w}_F(x+u) \equiv w(x)$. Physically, this accounts for the deflection

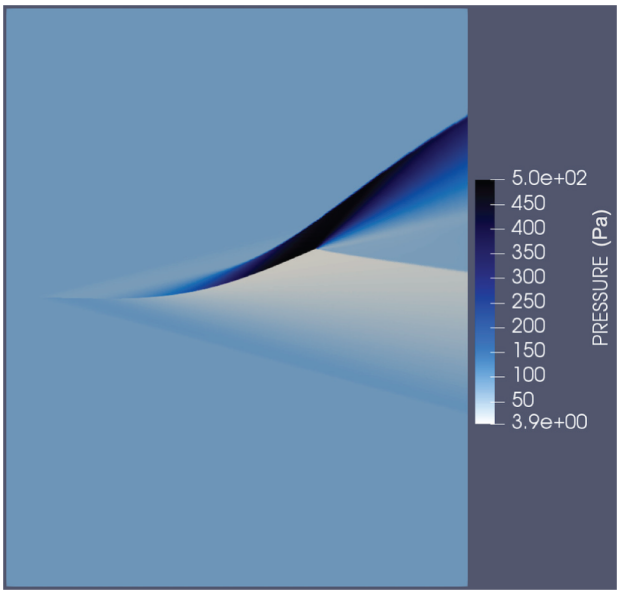

Fig. 10 Pressures calculated from Euler solution at maximum deflection, $\Lambda = 71.75$.

¶It is important to note that this Piston Theory limit occurs before the upper limit of structural deflection due to the constraints of the structural beam model itself. The beam model uses an approximation to derive the potential energy function which assumes that the slope in w is limited to values less than about 1/2. See Refs. [9,15] for details.

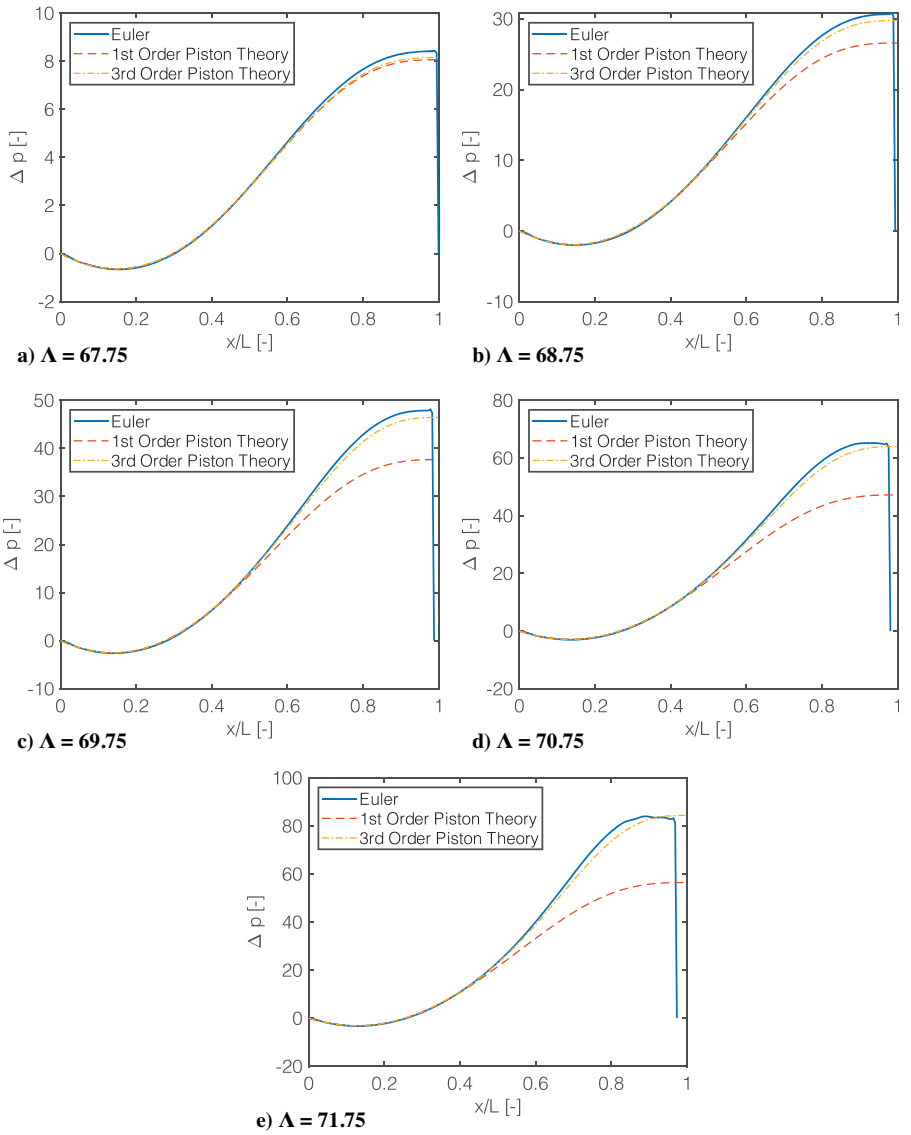

Fig. 11 Change in pressure across the beam length calculated by Euler, first-order Piston Theory, and third-order Piston Theory for various levels of Λ.

of the beam including the u deflections in the Euler case. Note that because $u(L)$ is negative the limits of integration are smaller for the Euler case than for the Piston Theory cases, which results in slightly more work done by third-order Piston Theory than that of Euler at large deflections, despite the pressures being similar.

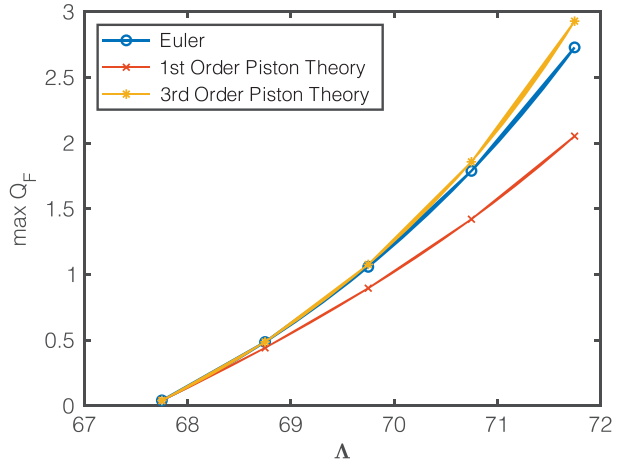

Fig. 12 Aerodynamic work done on the beam for various fluid forcing levels.

Figure 13 illustrates a representative plot of the change in pressure across the beam at a point at 80% of the beam length. Figure 13a shows one full deflection period in time, and Fig. 13b shows the Fourier transform of pressure, which illuminates the higher-frequency behavior.

It can be seen from these figures that pressures from all three theories align at small deflections but differ at larger forcing functions and deflections. Indeed, in Fig. 12, at a value of $\Lambda = 67.75$ (where the rms tip deflection is small), the aerodynamic work values all differ by only about 2.5%. As the forcing function and thus the deflections increase, first-order Piston Theory begins to differ from Euler, and, finally, all three differ at the highest forcing levels. Additionally, Fig. 13b shows that first-order Piston Theory does not capture higher modal content, but third-order Piston Theory and Euler do.

The good agreement for the aerodynamic pressure loading on the structure between the Euler model and third-order Piston Theory is reassuring and perhaps to some a pleasant surprise. However, it can be shown formally that the flutter point per se is the same whether one uses a linear potential flow theory or the Euler model if the mean flow is uniform as is the case here. A more interesting and challenging study would be to include the effect of a fluid boundary layer either using the shear flow model proposed by Lighthill [18] and adapted to the flutter of plates by Dowell [32] or to use a viscous CFD model, for example, Reynolds-averaged Navier–Stokes (RANS) or direct numerical simulation (DNS).

Finally, it is interesting to note a subtle difference between Figs. 4 and 12. That is, the fully coupled aeroelastic results show that

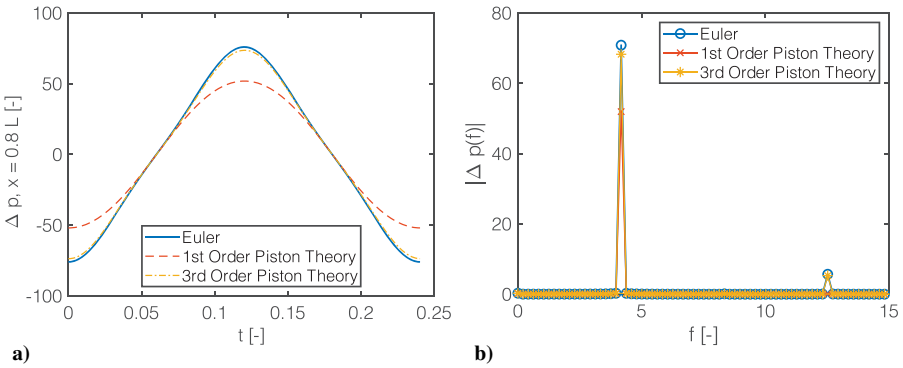

a) b)

Fig. 13 Change in pressure at 80% beam length in a) time space and b) frequency space.

first-order and third-order Piston Theory aerodynamics result in a relatively large difference in deflections, while the aerodynamic results of Fig. 12 show that the aerodynamic work is relatively close between the two theories, especially at small deflections. This indicates that the fully aeroelastic solver is sensitive to changes in the aerodynamic model.

VI. Conclusions

When modeling any physical system and certainly a fluid–structural (aeroelastic) system, it is important to study the sensitivity of the results. Three types of sensitivities have been identified and are explored in the present Paper. Type 1 is the sensitivity to the mathematical model of the physical system. Type 2 is that to the parameters that appear in the mathematical model or which are considered in the design of an experimental model. Type 3 is the accuracy of the numerical methods employed to extract solutions from the mathematical model.

The Type 3 sensitivity to the numerical solution method is considered by performing a convergence study to ensure that a sufficient number of structural modes are using in the computation and that the time step in the time-marching scheme is sufficiently small.

The Type 2 sensitivity to the parameters of the mathematical/physical system is addressed by first identifying the essential nondimensional parameters of the model. For the model considered here, there are three such nondimensional parameters. They are Λ, a ratio of aerodynamic forces to structural stiffness; μ, a ratio of fluid to structural mass; and M_∞, the Mach number. Indeed, if the first-order Piston Theory aerodynamic model is used, then only two parameters appear, namely, Λ and μ; in other words, the Mach number does not appear explicitly as an independent parameter but is included implicitly in the definitions of Λ and μ. On the other hand, if the third-order Piston Theory is used, then M_∞ appears as an independent parameter. The current example also illustrates a more general point, namely, that the number of essential nondimensional parameters depends on the mathematical/physical model adopted and the choice of these parameters (based upon a thorough analysis of the model and model results) can be such as to reduce the sensitivity of the model to the parameters. For example, it is found that the results are much less sensitive to μ than to Λ and also by incorporating M_∞ into Λ and μ the sensitivity to M_∞ can also be reduced. On the other hand, it is good to remember that the basic mathematical/physical model is only valid for a certain range of parameters. For example, in the present model, the Mach number must be sufficiently large compared to 1 for Piston Theory to be valid. How large is to some degree in the judgement of the analyst, but most investigators would say $M_\infty > 2$ should suffice. But then, if M_∞ is too large, other physical effects such as chemical reactions of the flow might be important, or the effects of fluid viscosity might be important even at lower M_∞, and these are neglected in the present aerodynamic model. Also, it is shown that, even without these additional physical effects, the (third-order) Piston Theory fails when the LCO response becomes too large, in other words, $M_\infty w/L > 1$.

Finally, even within the framework of the present mathematical/physical model, there are various physical effects that have greater or less impact on the model. That is, there is type 1 sensitivity in the model to whether a completely linear theory is used or whether the effects of structural stiffness or inertial nonlinearity is included in the model. Also, whether the effect of aerodynamic pressure acting normal to the instantaneous position of the mode is included (the β effect) or whether first- or third-order Piston Theory is included. All of these effects have been considered and discussed here. Indeed, this discussion of the Piston Theoretic pressures compared to Euler pressures shows that the aeroelastic solution is highly dependent on the aerodynamic model and therefore that third-order Piston Theory is more appropriate for this configuration than first order.

Looking ahead, one can note several future topics which may be explored. First, a fully coupled aeroelastic solution using an inviscid Euler code may validate the current model's structural motion prediction, because the model has been shown to be sensitive to small perturbations for certain parameters. Also, because of symmetry of the flow over the structure, the second-order aerodynamic terms from Piston Theory are omitted in this Paper but could be important for other related configurations, for example, flow over only one side of the structure or a structure with initial curvature or angle of attack. In addition, this Paper uses formulations for Piston Theory from Lighthill [18], whereas similar but more accurate descriptions of pressures on an oscillating piston surface are given by Liepmann and Roshko [29]. It is of some interest to develop a more complete Piston Theory using the latter formulations alongside the β effect. In addition, a study of the viscous and thermal effects may be of interest. Finally, a study using nonlinear plate theory (developed by the authors and collaborators [9,11]) for the structural model and this newly developed Piston Theory with follower effects for the aerodynamic model would also be valuable.

Appendix: Modal Equations and Typical Modal Physical Properties

A. Modal Equations

To derive the equations of motion for the beam, Lagrange's equations are used,

$$\frac{\partial}{\partial t}\frac{\partial \mathcal{L}}{\partial \dot{q}_n} - \frac{\partial \mathcal{L}}{\partial q_n} = Q_n \tag{A1}$$

where

$$\mathcal{L} = T - V + \int_0^L \lambda f \, \mathrm{d}x \tag{A2}$$

and Q_n is known from

$$\delta W^{NC} = \sum_n Q_n \delta q_n \tag{A3}$$

and the modal expansions are

$$u(x,t) = \sum_i \Psi_i^u(x) u_i(t) \tag{A4}$$

$$w(x,t) = \sum_j \Psi_j^w(x) w_j(t) \tag{A5}$$

$$\lambda(x,t) = \sum_k \Psi_k^\lambda(x) \lambda_k(t) \tag{A6}$$

Given dimensionally in Ref. [14], the equations of motion are as follows:

$$0 = m \int_0^L \Psi_i^u \Psi_i^u \, \mathrm{d}x \ddot{u}_i - \sum_k \lambda_k \int_0^L \Psi_i^{u'} \Psi_k^\lambda \, \mathrm{d}x \tag{A7}$$

$$\begin{aligned} 0 = {} & m \int_0^L \Psi_j^w \Psi_j^w \, \mathrm{d}x \ddot{w}_j + 2m\zeta_j \omega_j \int_0^L \Psi_j^w \Psi_j^w \, \mathrm{d}x \dot{w}_j \\ & + \omega_j^2 m \int_0^L \Psi_j^w \Psi_j^w \, \mathrm{d}x w_j - \sum_k \sum_{j1} \int_0^L \Psi_k^\lambda \Psi_{j1}^{w'} \Psi_j^{w'} \, \mathrm{d}x \lambda_k w_{j1} \\ & + EI \sum_{j1} \sum_{j2} \sum_{j3} \int_0^L (\Psi_{j1}^{w''} \Psi_{j2}^{w''} \Psi_{j3}^{w'} \Psi_j^{w'} \\ & + \Psi_{j1}^{w''} \Psi_{j2}^{w'} \Psi_{j3}^{w'} \Psi_j^{w''}) \, \mathrm{d}x w_{j1} w_{j2} w_{j3} \end{aligned} \tag{A8}$$

$$0 = \sum_i u_i \int_0^L \Psi_k^\lambda \Psi_i^{u'} \, \mathrm{d}x + \frac{1}{2} \sum_{j1} \sum_{j2} w_{j1} w_{j2} \int_0^L \Psi_k^\lambda \Psi_{j1}^{w'} \Psi_{j2}^{w'} \, \mathrm{d}x \tag{A9}$$

The system of equations now can be nondimensionalized as follows. First, consider Eq. (A7),

$$\begin{aligned} 0 &= mL\boldsymbol{M_u} \frac{EI}{mL^3} \ddot{\boldsymbol{u}} - \boldsymbol{A} \frac{EI}{L^2} \boldsymbol{\lambda} \\ 0 &= \boldsymbol{M_u} \ddot{\boldsymbol{u}} - \boldsymbol{A\lambda} \\ 0 &= \ddot{\boldsymbol{u}} - \boldsymbol{A\lambda} \end{aligned} \tag{A10}$$

Here, the final simplification is true if we normalize the modes such that $\boldsymbol{M_u} = I$.

Next, consider Eq. (A8),

$$\begin{aligned} 0 &= mL\boldsymbol{M_w} \frac{EI}{mL^3} \ddot{\boldsymbol{w}} + 2m\boldsymbol{\zeta} \left(\frac{EI}{mL^4}\right)^{1/2} \boldsymbol{\omega} L \boldsymbol{M_w} \left(\frac{EI}{mL^4}\right)^{1/2} L \dot{\boldsymbol{w}} \\ &\quad + \left(\frac{EI}{mL^4}\right) \boldsymbol{\omega}^2 mL \boldsymbol{M_w} L \boldsymbol{w} - \left(\frac{EI}{L^2}\right) L^{-1} \boldsymbol{B} L \boldsymbol{w\lambda} + \left(\frac{EI}{L^5}\right) \boldsymbol{P} L^3 \boldsymbol{www} \\ 0 &= \boldsymbol{M_w} \frac{EI}{L^2} \ddot{\boldsymbol{w}} + 2\boldsymbol{\zeta} \left(\frac{EI}{L^2}\right) \boldsymbol{\omega} \boldsymbol{M_w} \dot{\boldsymbol{w}} + \left(\frac{EI}{L^2}\right) \boldsymbol{\omega}^2 \boldsymbol{M_w} \boldsymbol{w} \\ &\quad - \left(\frac{EI}{L^2}\right) \boldsymbol{Bw\lambda} + \left(\frac{EI}{L^2}\right) \boldsymbol{Pwww} \\ 0 &= \boldsymbol{M_w} \ddot{\boldsymbol{w}} + 2\boldsymbol{\zeta\omega} \boldsymbol{M_w} \dot{\boldsymbol{w}} + \boldsymbol{\omega}^2 \boldsymbol{M_w} \boldsymbol{w} - \boldsymbol{Bw\lambda} + \boldsymbol{Pwww} \\ 0 &= \ddot{\boldsymbol{w}} + 2\boldsymbol{\zeta\omega} \dot{\boldsymbol{w}} + \boldsymbol{\omega}^2 \boldsymbol{w} - \boldsymbol{Bw\lambda} + \boldsymbol{Pw}^3 \end{aligned} \tag{A11}$$

where again the final step is true if $\boldsymbol{M_w} = I$.

Lastly, consider Eq. (A9),

$$\begin{aligned} 0 &= \boldsymbol{AL u} + \frac{1}{2L} \boldsymbol{B} L^2 \boldsymbol{ww} \\ 0 &= \boldsymbol{Au} + \frac{1}{2} \boldsymbol{Bww} \\ 0 &= \boldsymbol{u} + \frac{1}{2} \boldsymbol{A}^{-1} \boldsymbol{Bww} \end{aligned} \tag{A12}$$

Summarizing, we can succinctly write the unforced equations of motion, rearranging the zeros on the right-hand side to signify the absence of forcing:

$$\ddot{\boldsymbol{u}} - \boldsymbol{A\lambda} = 0 \tag{A13}$$

$$\ddot{\boldsymbol{w}} + 2\boldsymbol{\zeta\omega} \dot{\boldsymbol{w}} + \boldsymbol{\omega}^2 \boldsymbol{w} - \boldsymbol{Bw\lambda} + \boldsymbol{Pw}^3 = 0 \tag{A14}$$

$$\boldsymbol{u} + \frac{1}{2} \boldsymbol{A}^{-1} \boldsymbol{Bww} = 0 \tag{A15}$$

B. Typical Model Physical Properties

Structural properties are

$$\begin{aligned} b &= 0.04 \text{ m} \\ h &= 0.0001 \text{ m}; \\ L &= 0.1 \text{ m}; \\ \rho &= 2770 \text{ kg/m}^3; \\ E &= 71 \times 10^9 \text{ Pa}; \\ I &= bh^3/(12(1 - 0.33^2)); \\ EI &= E * I; \\ m &= \rho bh \end{aligned}$$

Air properties are

$$\begin{aligned} 112 < T_\infty &< 120 \text{ K} \\ R &= 287.058 \text{ J/(kg} \cdot \text{K)} \\ \gamma &= 1.4 \\ 2 \le M_\infty &\le 6 \\ 74 \le p_\infty &\le 81 \text{ N/m}^2 \end{aligned}$$

Acknowledgments

The first author's graduate studies are supported by the Department of Defense SMART Scholarship. The fourth author acknowledges the support of the U.S. Air Force Office of Scientific Research through funding received from the Computational Mathematics program (Fahroo, Program Officer). This Paper is also funded in part by an AFOSR grant from program director Jaimie Tiley. The authors would like thank Tiley and Ivett Leyva for their counsel and guidance. This paper is approved for public release, distribution unlimited (88ABW-2019-5242).

References

[1] Spottswood, S. M., Beberniss, T. J., Eason, T. G., Perez, R. A., Donbar, J. M., Ehrhardt, D. A., and Riley, Z. B., "Exploring the Response of a Thin, Flexible Panel to Shock-Turbulent Boundary-Layer Interactions," *Journal of Sound Vibration*, Vol. 443, March 2019, pp. 74–89. https://doi.org/10.1016/j.jsv.2018.11.035

[2] Freydin, M., Dowell, E. H., Whalen, T. J., and Laurence, S. J., "A Theoretical Computational Model of a Plate in Hypersonic Flow," *Journal of Fluids and Structures*, Vol. 93, Feb. 2020, Paper 102858. https://doi.org/10.1016/j.jfluidstructs.2019.102858

[3] Currao, G. M. D., Neely, A. J., Kennell, C. M., Gai, S. L., and Buttsworth, D. R., "Hypersonic Fluid–Structure Interaction on a Cantilevered Plate with Shock Impingement," *AIAA Journal*, Vol. 57, No. 11, 2019, pp. 4,819–4,834. https://doi.org/10.2514/1.J058375

[4] Lacarbonara, W., *Nonlinear Structural Mechanics: Theory, Dynamical Phenomena, and Modeling*, Springer, New York, 2013, pp. 292–368.

[5] Lacarbonara, W., and Yabuno, H., "Refined Models of Elastic Beams Undergoing Large In-Plane Motions: Theory and Experiment," *International Journal of Solids and Structures*, Vol. 43, No. 17, 2006, pp. 5066–5084. https://doi.org/10.1016/j.ijsolstr.2005.07.018

[6] Hamdan, M., and Dado, M., "Large Amplitude Free Vibrations of a Uniform Cantilever Beam Carrying an Intermediate Lumped Mass and

Rotary Inertia," *Journal of Sound and Vibration*, Vol. 206, No. 2, 1997, pp. 151–168.
https://doi.org/10.1006/jsvi.1997.1081

[7] Crespo da Silva, M., and Glynn, C., "Non-Linear Flexural-Flexural-Torsional Dynamics of Inextensional Beams. I. Equations of Motion," *Journal of Structural Mechanics*, Vol. 6, No. 4, 1978, pp. 437–448.
https://doi.org/10.1080/03601217808907348

[8] Crespo da Silva, M., and Glynn, C., "Non-Linear Flexural-Flexural-Torsional Dynamics of Inextensional Beams. II. Forced Motions," *Journal of Structural Mechanics*, Vol. 6, No. 4, 1978, pp. 449–461.
https://doi.org/10.1080/03601217808907349

[9] Tang, D., Zhao, M., and Dowell, E., "Inextensible Beam and Plate Theory: Computational Analysis and Comparison with Experiment," *Journal of Applied Mechanics*, Vol. 81, No. 6, 2014, Paper 061009.
https://doi.org/10.1115/1.4026800

[10] Tang, D., Gibbs, S., and Dowell, E., "Nonlinear Aeroelastic Analysis with Inextensible Plate Theory Including Correlation with Experiment," *AIAA Journal*, Vol. 53, No. 5, 2015, pp. 1299–1308.
https://doi.org/10.2514/1.J053385

[11] Dowell, E., and McHugh, K., "Equations of Motion for an Inextensible Beam Undergoing Large Deflections," *Journal of Applied Mechanics*, Vol. 83, May 2016, Paper 051007.
https://doi.org/10.1115/1.4032795

[12] Raviv Sayag, M., and Dowell, E., "Linear Versus Nonlinear Response of a Cantilevered Beam Under Harmonic Base Excitation: Theory and Experiment," *Journal of Applied Mechanics*, Vol. 83, Oct. 2016, Paper 101002.
https://doi.org/10.1115/1.4034117

[13] McHugh, K., and Dowell, E., "Nonlinear Responses of Inextensible Cantilever and Free-Free Beams Undergoing Large Deflections," *Journal of Applied Mechanics*, Vol. 85, May 2018, Paper 051008.
https://doi.org/10.1115/1.4039478

[14] McHugh, K. A., and Dowell, E. H., "Nonlinear Response of an Inextensible, Cantilevered Beam Subjected to a Nonconservative Follower Force," *Journal of Computational and Nonlinear Dynamics*, Vol. 14, No. 3, 2019, Paper 031004.
https://doi.org/10.1115/1.4042324

[15] Culver, D., McHugh, K., and Dowell, E., "An Assessment and Extension of Geometrically Nonlinear Beam Theories," *Mechanical Systems and Signal Processing*, Vol. 134, Dec. 2019, Paper 106340.
https://doi.org/10.1016/j.ymssp.2019.106340

[16] Beck, M., "Die Knicklast des einseitig eingespannten, tangential gedrückten Stabes," *Zeitschrift für angewandte Mathematik und Physik ZAMP*, Vol. 3, May 1952, pp. 225–228.
https://doi.org/10.1007/BF02008828

[17] Hayes, W., and Probstein, R., *Hypersonic Flow Theory*, Academic Press, New York, 1959, Chap. 2.

[18] Lighthill, M., "Oscillating Airfoils at High Mach Number," *Journal of the Aeronautical Sciences*, Vol. 20, June 1953, pp. 402–406.
https://doi.org/10.2514/8.2657

[19] Ashley, H., and Zartarian, G., "Piston Theory—A New Aerodynamic Tool for the Aeroelastician," *Journal of the Aeronautical Sciences*, Vol. 23, Dec. 1956, pp. 1109–1118.
https://doi.org/10.2514/8.3740

[20] Nydick, I., Friedmann, P. P., and Zhong, X., "Hypersonic Panel Flutter Studies on Curved Panels," AIAA Paper 1995-1485, 1995.
https://doi.org/10.2514/6.1995-1485

[21] Dowell, E. H., et al., *A Modern Course in Aeroelasticity*, Springer, New York, 2015, pp. 91–92, 170–184.
https://doi.org/10.1007/978-3-319-09453-3

[22] McNamara, J. J., Crowell, A. R., Friedmann, P. P., Glaz, B., and Gogulapati, A., "Approximate Modeling of Unsteady Aerodynamics for Hypersonic Aeroelasticity," *Journal of Aircraft*, Vol. 47, No. 6, Nov.–Dec. 2010, pp. 1932–1945.
https://doi.org/10.2514/1.C000190

[23] Scott, R. C., and Pototzky, A. S., "Quasisteady Aerodynamics for Flutter Analysis Using Steady Computational Fluid Dynamics Calculations," *Journal of Aircraft*, Vol. 33, No. 1, 1996, pp. 191–197.
https://doi.org/10.2514/3.46921

[24] Zhang, W.-W., Ye, Z.-Y., Zhang, C.-A., and Liu, F., "Supersonic Flutter Analysis Based on a Local Piston Theory," *AIAA Journal*, Vol. 47, No. 10, 2009, pp. 2321–2328.
https://doi.org/10.2514/1.37750

[25] Meijer, M.-C., and Dala, L., "Role of Higher-Order Terms in Local Piston Theory," *Journal of Aircraft*, Vol. 56, No. 1, 2019, pp. 388–391.
https://doi.org/10.2514/1.C034920

[26] Brouwer, K. R., and McNamara, J. J., "Enriched Piston Theory for Expedient Aeroelastic Loads Prediction in the Presence of Shock Impingements," *AIAA Journal*, Vol. 57, No. 3, 2019, pp. 1288–1302.
https://doi.org/10.2514/1.J057595

[27] Shi, X., Tang, G., Yang, B., and Li, H., "Supersonic Flutter Analysis of Vehicles at Incidence Based on Local Piston Theory," *Journal of Aircraft*, Vol. 49, No. 1, 2012, pp. 333–337.
https://doi.org/10.2514/1.C031465

[28] Meng, X., Ye, Z., Ye, K., and Liu, C., "Aerodynamic Nonlinearity of Piston Theory in Surface Vibration," *Journal of Aerospace Engineering*, Vol. 33, No. 4, 2020, Paper 04020035.
https://doi.org/10.1061/(ASCE)AS.1943-5525.0001148

[29] Liepmann, H., and Roshko, A., *Elements of Gas Dynamics*, Wiley, New York, 1957, Chap. 3.

[30] Dowell, E. H., and Bliss, D. B., "New Look at Unsteady Supersonic Potential Flow Aerodynamics and Piston Theory," *AIAA Journal*, Vol. 51, No. 9, 2013, pp. 2278–2281.
https://doi.org/10.2514/1.J052088

[31] Dowell, E. H., and Bliss, D. B., "New Look at Unsteady Supersonic Potential Flow Aerodynamics and Piston Theory," *AIAA Journal*, Vol. 53, No. 8, 2015, pp. 2419–2419.
https://doi.org/10.2514/1.J054540

[32] Dowell, E., *Aeroelasticity of Plates and Shells*, Springer Netherlands, Leyden, The Netherlands, 1975, pp. 57–64.